

Shielding Effectiveness of Multiple-Shield Cables with Arbitrary Terminations via Transmission Line Analysis

Salvatore Campione*, Lorena I. Basilio, Larry K. Warne,
H. Gerald Hudson, and William L. Langston

Abstract—In this paper we report on a transmission-line model for calculating the shielding effectiveness of multiple-shield cables with arbitrary terminations. Since the shields are not perfect conductors and apertures in the shields permit external magnetic and electric fields to penetrate into the interior regions of the cable, we use this model to estimate the effects of the outer shield current and voltage (associated with the external excitation and boundary conditions associated with the external conductor) on the inner conductor current and voltage. It is commonly believed that increasing the number of shields of a cable will improve the shielding performance. However, this is not always the case, and a cable with multiple shields may perform similar to or in some cases worse than a cable with a single shield. We want to shed more light on these situations, which represent the main focus of this paper.

1. INTRODUCTION

Protecting a device from coupling of an external electromagnetic environment through a cable shield is at times a formidable task. Early work on solid shields can be found in Schelkunoff's paper [1], and valuable information on cables and shielding can be found in various textbooks [2–5]. Shielding effectiveness is a common quantity that represents the shielding performance, measured as the reduction of the electromagnetic field at a given point in space (e.g., at a point in the inner conductor in the case of a cable) caused by placing a shield between the source and that point. Early works on shielding effectiveness of cables can be found in [6–8]. It is generally thought that increasing the number of shields of a cable will improve the shielding performance [9, 10]. However, there are situations in which a cable with multiple shields may perform similar to or worse than a cable with a single shield, and this has been seldom discussed in literature.

To address the question of shielding effectiveness in multiple-shield cables, we rigorously formulate a transmission-line model for determining the shielding effectiveness of such cables in the presence of arbitrary terminations. We assume the presence of an external excitation that produces the outer shield current and voltage which, in turn, induces the internal currents and voltages on the inner shield(s) and conductor. This non-zero transfer function results because the shields are not perfect conductors and apertures in the shields permit external magnetic and electric fields to penetrate into the interior region of the cable. We will analyze various cable configurations with varying numbers of shields and termination loads, whose shielding effectiveness will be compared. This cable survey will highlight the fact that cables with multiple shields may at times not exhibit much improvement relative to single-shield cables (and in certain frequency regions perform worse than single-shield cables), possibly not providing the extra protection desired.

Received 24 March 2016, Accepted 12 June 2016, Scheduled 25 June 2016

* Corresponding author: Salvatore Campione (sncampi@sandia.gov).

The authors are with the Electromagnetic Theory Department, Sandia National Laboratories, P. O. Box 5800, Albuquerque, NM 87185, USA.

2. TRANSMISSION-LINE MODEL OF MULTIPLE-SHIELD CABLES WITH ARBITRARY TERMINATIONS

2.1. Case of a Single Shield

In order to model a shielded cable, we consider an element of transmission line of differential length dz that contains a distributed voltage source $E_z(z) = Z_T I_0(z)$, where $I_0(z)$ is the current on the outer shield, as well as a distributed current source $J_z(z) = -Y_T V_0(z)$, where $V_0(z)$ is the external voltage on the outer shield. For reference, the external and internal electrical quantities for a shielded cable are labeled in Fig. 1(a). The shield properties (related to the braid weave characteristics and material) are accounted for in the per-unit length transfer impedance Z_T and transfer admittance Y_T . More specifically, these terms capture the magnetic and electric field coupling mechanisms from the exterior of the cable to the inner conductor. For the purposes of this paper, it is assumed that these quantities are known (and determined from the particular braid characteristics [11–13]) and can be directly incorporated into the transmission-line model.

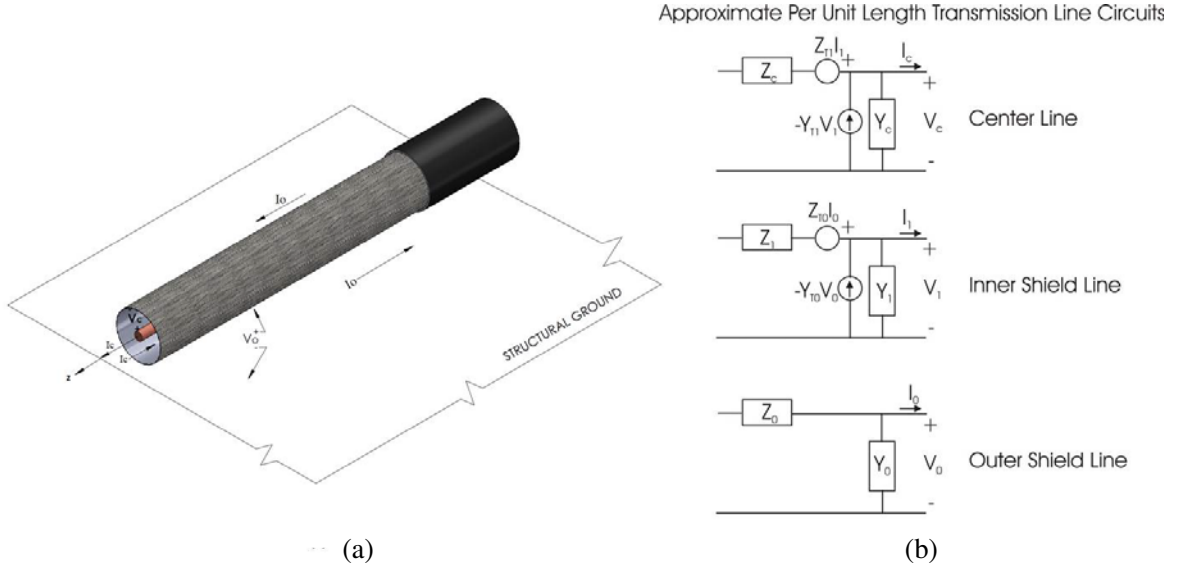


Figure 1. (a) Voltages and currents associated with shielded cable analysis. (b) Approximate per-unit-length transmission line circuits for the double-shield cable case.

The differential equations for the voltage and current on the inner conductor of the braided cable (V_c and I_c) are given by

$$\frac{dV_c}{dz} + Z_c I_c = Z_T I_0(z) \quad \frac{dI_c}{dz} + Y_c V_c = -Y_T V_0(z). \quad (1)$$

In addition to the transfer parameters associated with the external cable characteristics, Eq. (1) also contains the per-unit length (series) self-impedance Z_c and (shunt) self-admittance Y_c , which are formed by the inner conductor and the shield. As with the transfer impedance and transfer admittance, it will be assumed in this paper that the self-parameters characterizing the shielded cable geometry are known. From Eq. (1), it is clear that the sources for the transmission line are defined by the transfer parameters of the shielded cable and that these sources drive the coupled voltage and current on the inner conductor of the cable. At this point, we rewrite the second differential equation in Eq. (1) in a generalized form that allows for cases when the braided cable is located within an arbitrary structure such as a metallic cavity of arbitrary shape. In other words, we recognize that there may be situations where the exterior voltage $V_0(z)$ is not easily defined. Relating the transfer admittance Y_T to the transfer capacitance C_T , we can write

$$\frac{dI_c}{dz} + Y_c V_c = -j\omega C_T V_0(z) = -j\omega C_T \frac{q_0(z)}{C_0}, \quad (2)$$

where $q_0(z)$ and C_0 represent the charge and capacitance per-unit length of the outer shield, respectively. Since the transfer capacitance is proportional to the outer capacitance C_0 , Eq. (2) can also be expressed as

$$\frac{dI_c}{dz} + Y_c V_c = -j\omega \tilde{C}_T q_0(z), \quad (3)$$

where \tilde{C}_T is the transfer capacitance normalized by C_0 . Using the current continuity equation $\nabla \cdot \vec{j} = -j\omega \rho_0$ or equivalently $\frac{dI_0}{dz} = -j\omega q_0(z)$, Eq. (3) becomes

$$\frac{dI_c}{dz} + Y_c V_c = \tilde{C}_T \frac{dI_0(z)}{dz}. \quad (4)$$

Note that with the first differential equation in Eq. (1) and Eq. (4), the interior voltage and current can be found directly from the exterior cable current $I_0(z)$ (and its derivative) and the transfer parameters characterizing the braided shield.

To solve the interior system of Eqs. (1) and (4), we will consider one source at a time and then apply a superposition of results for the final value of the inner conductor current [2]. Thus, assuming $J_z(z) = \tilde{C}_T \frac{dI_0(z)}{dz} = 0$ and using Eq. (1), the second-order differential equation for the inner conductor current becomes

$$\left(\frac{d^2}{dz^2} - \gamma_c^2 \right) I_c = -Y_c E_z(z) = -Y_c Z_T I_0(z), \quad (5)$$

where $\gamma_c^2 = Z_c Y_c$. The solution of Eq. (5) is given by

$$\begin{aligned} I_{c,e}(z) &= [K_{1,e} + P_e(z)] e^{-\gamma_c z} + [K_{2,e} + Q_e(z)] e^{\gamma_c z} \\ V_{c,e}(z) &= \sqrt{\frac{Z_c}{Y_c}} \{ [K_{1,e} + P_e(z)] e^{-\gamma_c z} - [K_{2,e} + Q_e(z)] e^{\gamma_c z} \}, \end{aligned} \quad (6)$$

with $P_e(z) = \frac{1}{2} \sqrt{\frac{Y_c}{Z_c}} \int_{z_-}^z e^{\gamma_c z} E_z(z) dz$ and $Q_e(z) = \frac{1}{2} \sqrt{\frac{Y_c}{Z_c}} \int_z^{z_+} e^{-\gamma_c z} E_z(z) dz$, with $E_z(z) = Z_T I_0(z)$. The constants in Eq. (6) are determined from the terminating impedances $Z_{L,c}^-$ and $Z_{L,c}^+$ to the interior transmission line (at locations z_- and z_+ , respectively, where $z_- < z < z_+$). More specifically,

$$\begin{aligned} K_{1,e} &= \rho_- e^{\gamma_c z_-} \frac{\rho_+ P_e(z_+) e^{-\gamma_c z_+} - Q_e(z_-) e^{\gamma_c z_+}}{e^{\gamma_c(z_+ - z_-)} - \rho_- \rho_+ e^{-\gamma_c(z_+ - z_-)}} \\ K_{2,e} &= \rho_+ e^{-\gamma_c z_+} \frac{\rho_- Q_e(z_-) e^{\gamma_c z_-} - P_e(z_+) e^{-\gamma_c z_-}}{e^{\gamma_c(z_+ - z_-)} - \rho_- \rho_+ e^{-\gamma_c(z_+ - z_-)}}, \end{aligned} \quad (7)$$

where the reflection coefficients at positions z_- and z_+ are $\rho_- = \frac{Z_{L,c}^- - \sqrt{\frac{Z_c}{Y_c}}}{Z_{L,c}^- + \sqrt{\frac{Z_c}{Y_c}}}$ and $\rho_+ = \frac{Z_{L,c}^+ - \sqrt{\frac{Z_c}{Y_c}}}{Z_{L,c}^+ + \sqrt{\frac{Z_c}{Y_c}}}$.

With Eq. (6) accounting for the interior current driven by magnetic coupling and diffusion of the exterior field into the inner conductor, we now move on to accounting for the current contribution associated with the electric coupling of the exterior field. For this case, we assume $E_z(z) = 0$ so that we obtain (where we have used the second differential equation in Eq. (12) with $Y_0 = j\omega C_0$)

$$\left(\frac{d^2}{dz^2} - \gamma_c^2 \right) V_c = -Z_c \tilde{C}_T \frac{dI_0(z)}{dz}, \quad (8)$$

and thus

$$\begin{aligned} V_{c,j}(z) &= [K_{1,j} + P_j(z)] e^{-\gamma_c z} + [K_{2,j} + Q_j(z)] e^{\gamma_c z} \\ I_{c,j}(z) &= \sqrt{\frac{Y_c}{Z_c}} \{ [K_{1,j} + P_j(z)] e^{-\gamma_c z} - [K_{2,j} + Q_j(z)] e^{\gamma_c z} \}, \end{aligned} \quad (9)$$

with $P_j(z) = \frac{1}{2} \sqrt{\frac{Z_c}{Y_c}} \int_{z_-}^z e^{\gamma_c z} J_z(z) dz$ and $Q_j(z) = \frac{1}{2} \sqrt{\frac{Z_c}{Y_c}} \int_z^{z_+} e^{-\gamma_c z} J_z(z) dz$, with $J_z(z) = -Y_T V_0(z)$, and

$$\begin{aligned} K_{1,j} &= \rho_- e^{\gamma_c z_-} \frac{Q_j(z_-) e^{\gamma_c z_+} + \rho_+ P_j(z_+) e^{-\gamma_c z_+}}{e^{\gamma_c(z_+ - z_-)} - \rho_- \rho_+ e^{-\gamma_c(z_+ - z_-)}} \\ K_{2,j} &= \rho_+ e^{-\gamma_c z_+} \frac{P_j(z_+) e^{-\gamma_c z_-} + \rho_- Q_j(z_-) e^{\gamma_c z_-}}{e^{\gamma_c(z_+ - z_-)} - \rho_- \rho_+ e^{-\gamma_c(z_+ - z_-)}}. \end{aligned} \quad (10)$$

Thus, to obtain the total current and voltage induced on the inner conductor we sum the two individual contributions:

$$\begin{aligned} I_c(z) &= I_{c,e}(z) + I_{c,j}(z) \\ V_c(z) &= V_{c,e}(z) + V_{c,j}(z). \end{aligned} \quad (11)$$

2.2. Case of Multiple Shields

Cables with more than one shield can be analyzed by applying the transmission-line model shown in Sec. 2.1 to each shield to obtain the current in the next shield until all shields have been accounted for. Assuming N shields, the outer to inner shields to be indexed as $0, 1, 2, \dots, N-1$, the differential equations for the voltage and current on the 0^{th} shield (outermost shield) are given by

$$\frac{dV_0}{dz} + Z_0 I_0 = Z_{T,0} I_1, \quad \frac{dI_0}{dz} + Y_0 V_0 = -Y_{T,0} V_1. \quad (12)$$

In what follows, we neglect the interaction from the cable to the driving circuit using the weak coupling assumption, i.e., $Z_{T,0} I_1 = 0$ and $Y_{T,0} V_1 = 0$. If the weak coupling assumption is not valid, the solution of the differential equations can be obtained although it is more complex. Thus, we assume that the current distribution on the outermost shield $I_0(z)$ is known.

The internal problem is now set by looking at the i^{th} internal shield, with $i = 1, 2, \dots, N-1$, as

$$\begin{aligned} \frac{dV_i}{dz} + Z_i I_i &= Z_{T,(i-1)} I_{(i-1)} + Z_{T,i} I_{(i+1)} \\ \frac{dI_i}{dz} + Y_i V_i &= \tilde{C}_{T,(i-1)} \frac{dI_{(i-1)}}{dz} + \tilde{C}_{T,i} \frac{dI_{(i+1)}}{dz} \end{aligned} \quad (13)$$

Again, we will neglect the interaction from the cable to the driving circuit, i.e., $Z_{T,i} I_{(i+1)} = 0$ and $\tilde{C}_{T,i} \frac{dI_{(i+1)}}{dz} = 0$. From Eq. (13), it is clear that the sources for the i^{th} transmission line are defined by the transfer parameters of the $(i-1)^{th}$ shield and that these sources drive the coupled voltage and current on the interior shield. We highlight this fact in Fig. 1(b) where we report approximate per-unit-length transmission line circuits for the double-shield cable case.

We will again consider one source at a time and then apply a superposition of results for the final value of the interior current. Eq. (6) can be used to compute $I_{i,e}(z)$ and $V_{i,e}(z)$ as a result of the interior current driven by magnetic coupling and diffusion of the exterior field into the inner conductor, but now using the i^{th} shield parameters and $E_z(z) = Z_{T,(i-1)} I_{(i-1)}$. In a similar way, the required constants in Eq. (7) are now determined from the terminating impedances $Z_{L,i}^-$ and $Z_{L,i}^+$ to the interior transmission line (at locations z_- and z_+ , respectively, where $z_- < z < z_+$) using the i^{th} shield parameters.

In a similar manner, Eq. (9) can be used to compute $I_{i,j}(z)$ and $V_{i,j}(z)$ as a result of the current contribution associated with the electric coupling of the exterior field, but now using the i^{th} shield parameters and $J_z(z) = -Y_{T,(i-1)} V_{(i-1)}$. Similarly, the required constants in Eq. (10) are now determined from the terminating impedances $Z_{L,i}^-$ and $Z_{L,i}^+$ to the interior transmission line using the i^{th} shield parameters. Thus, to obtain the total current and voltage induced on the i^{th} internal shield we sum the two individual contributions as done in Eq. (11).

Finally, the differential equations for the voltage and current on the inner conductor of the braided cable (V_c and I_c) are given by

$$\begin{aligned} \frac{dV_c}{dz} + Z_c I_c &= Z_{T,(N-1)} I_{(N-1)} \\ \frac{dI_c}{dz} + Y_c V_c &= \tilde{C}_{T,(N-1)} \frac{dI_{(N-1)}}{dz}. \end{aligned} \tag{14}$$

From Eq. (14), it is clear that the sources for the innermost transmission line formed by the $(N - 1)^{th}$ shield and the inner conductor are defined by the transfer parameters of the $(N - 1)^{th}$ shield and that these sources drive the coupled voltage and current on the inner conductor of the cable. See Fig. 1(b) where this is reported for the double-shield cable case.

We will again consider one source at a time and then apply a superposition of results for the final value of the inner conductor current. Eq. (6) can be used to compute $I_{c,j}(z)$ and $V_{c,j}(z)$ as a result of magnetic coupling and diffusion of the exterior field into the inner conductor, but now using the inner conductor parameters and $E_z(z) = Z_{T,(N-1)} I_{(N-1)}$. In a similar way, the required constants in Eq. (7) are now determined from the terminating impedances $Z_{L,c}^-$ and $Z_{L,c}^+$ to the interior transmission line (at locations z_- and z_+ , respectively, where $z_- < z < z_+$) using the inner conductor parameters.

In a similar manner, Eq. (9) can be used to compute $I_{c,j}(z)$ and $V_{c,j}(z)$ as a result of the current contribution associated with the electric coupling of the exterior field, but now using the inner conductor parameters and $J_z(z) = -Y_{T,(N-1)} V_{(N-1)}$. Similarly, the required constants in Eq. (10) are now determined from the terminating impedances $Z_{L,c}^-$ and $Z_{L,c}^+$ to the interior transmission line using the inner conductor parameters. Thus, to obtain the total current and voltage induced on the inner conductor we sum the two individual contributions as done in Eq. (11).

3. NUMERICAL EXAMPLES

In this section, we will impose the distribution of the (outermost shield) disturbing current to be known and equal to $I_0(z) = I_0 e^{-\gamma_0 z}$. We will then estimate the shielding effectiveness as

$$SE(z) = 20 \log_{10} \frac{I_c(z)}{I_0(z)}. \tag{15}$$

We would like to stress that the definition in Eq. (15) also complies with the definition of ratio of current in the core with and without the shield. In our particular drive condition we are not looking to the response to an incident wave, but to a forced current source. Therefore, if the shield is removed, our drive condition would inject a current on the core conductor of known value $I_0(z)$; then, if we put the shield on, our drive condition would impose a known current on the shield and we would find the current on the core conductor $I_c(z)$. Then, we define shielding effectiveness as the ratio of the current in the center conductor in the second case (with shield) to the one in the first case (no shield). This is exactly the definition of shielding effectiveness as the ratio of current in the core with and without the shield.

We will also adopt the complete semi-empirical model assembled by Kley [11] based on measurements of typical commercial cables. More accurate models could be adopted, e.g., multipoles [12, 13], but they are not necessary for the effects we are interested in in this paper. Unless otherwise stated, we will assume a PEC inner conductor and braid for the description of Z_c and the propagation impedances; this assumption is not applied to the transfer parameters.

3.1. Single Shield Cable Analysis and Experimental Verification

Let's first consider the case of three 22-inch-long, commercial single shield cables, which differ for the level of optical coverage (from low to high): REMEE (59%), Belden 9201 (78%), and Belden 8240 (95%) [14]. The origin of the reference system is located at the center of the cable, so that $z = -11$ inch and $z = +11$ inch represent the two cable terminations. This will be valid also for the results in Sec. 3.2. We take the simulation parameters to be $Z_T = Z_R + j\omega L_T + Z_S$, where $Z_R = R_{gs} \frac{\gamma d_R}{\sin(\gamma d_R)}$

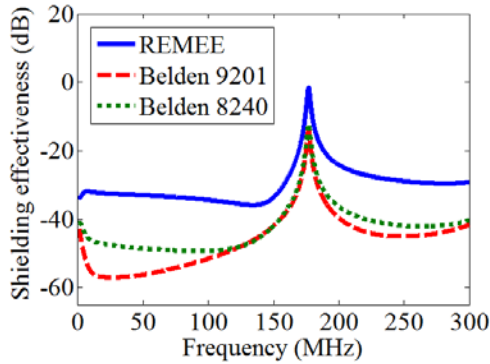


Figure 2. Shielding effectiveness for a 22-inch-long REMEE, Belden 9201, and Belden 8240 cable computed at $z = -11$ inch (the left termination end of the cable) assuming a load of 0.5Ω at the inner conductor transmission line.

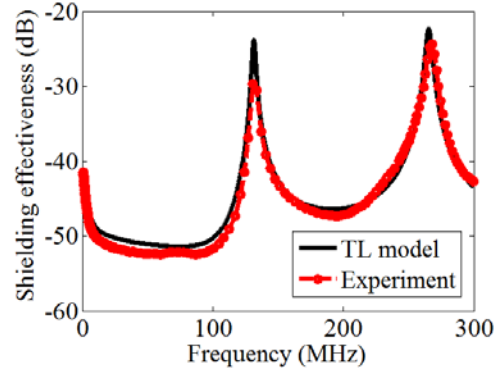


Figure 3. Comparison of measured and theoretical shielding effectiveness for a 22-inch-long Belden 8240 cable computed at the load side (at $z = -11$ inch).

Table 1. Simulation parameters for the load to model the experiment.

Frequency (MHz)	10	60	86	160	200	300
R_L (Ω)	0.50	0.60	0.70	1.00	1.25	2.80
L_L (nH)	25.7	25.7	25.7	27.0	28.0	32.0

accounts for the shield diffusion effect, with $\gamma = \frac{1-j}{\delta} = (1.21 - j1.21) \times 10^3 \sqrt{\omega/\omega_0}$ inch $^{-1}$, $\delta = \sqrt{\frac{2}{\omega\mu_0\sigma}} = 8.2 \times 10^{-4} \sqrt{\omega_0/\omega}$ inch the skin depth, $R_{gs} = \{34.28, 18.34, 13.34\}$ m Ω /m, and $d_R = \{3.68, 3.47, 3.5\} \times 10^{-3}$ inch for {REMEE, Belden 9201, Belden 8240}, $Z_S = (1 + j)\omega L_S$ is the internal transfer impedance assumed to be a forty five degree quantity, with $L_S = \{821, -217.6, -462.6\} \sqrt{\omega_0/\omega}$ pH/m for {REMEE, Belden 9201, Belden 8240}, $Y_T = j\omega C_T$, with $L_T = \{5614.6, -134.6, -754.9\}$ pH/m and $C_T = \{863.07, 177.9, 7.3\}$ fF/m for {REMEE, Belden 9201, Belden 8240}. We plot in Fig. 2 the shielding effectiveness computed at $z = -11$ inch (a termination end) assuming a load of 0.5Ω at both ends of the inner conductor transmission line for the three cables.

We observe a resonating behavior at around 175 MHz. A comparison of the three cables leads to the conclusion that the REMEE cable provides the lowest level of shielding, whereas the two Belden cables have comparable shielding effectiveness (with the Belden 9201 having slightly better performance at these frequencies). This result appears to be counterintuitive since the 8240 cable has a higher optical coverage leading one to believe that it should have better shielding performance. However, the shield topology of the Belden 9201 features near cancellation of the porpoising and hole effects [15], leading to better shielding effectiveness.

In order to provide confidence in our transmission-line model, we measure and report in Fig. 3 and Fig. 4 the shielding effectiveness of two 22-inch long Belden 8240 and Belden 9201 cables. In the experiment, we measure the current on the load as well as the current on the shield, with which we are able to determine the shielding effectiveness. To use the model described in Sec. 2, we should understand the experimental conditions. The current probes at the ends of the cable tester represent $Z_L \rightarrow 0.5\Omega$ loads at low frequencies. Near the resonance of the tester it was found that the loads exhibit increasing losses as well as reactive effects. Thus, to get a better understanding of these load values, several experiments were performed [16]. The load $Z_L = R_L + j\omega L_L$ has been approximated in simulation as a linear interpolation function with the parameters in Table 1. The presence of such reactive components leads to an overall frequency downshift with respect to the results shown in Fig. 2. We also included proper resistive components for the description of Z_c to account for cable attenuation [14], and R_c has

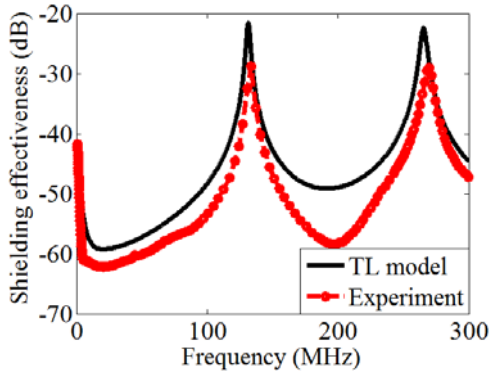


Figure 4. Comparison of measured and theoretical shielding effectiveness for a 22-inch-long Belden 9201 cable computed at the load side (at $z = -11$ inch).

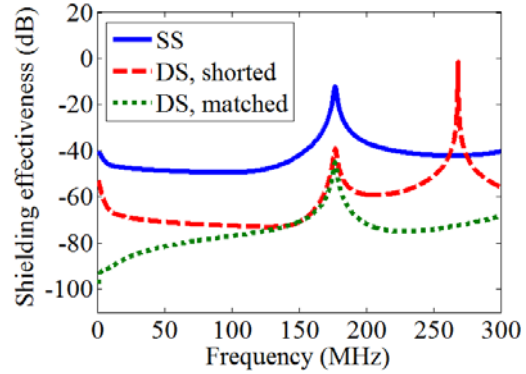


Figure 5. Shielding effectiveness for a 22-inch-long single and double-shield cable (referred to as SS and DS in the legend, respectively) computed at $z = -11$ inch assuming a load of 0.5Ω at the inner conductor transmission line. The inner shield transmission line is considered to be shorted or matched.

Table 2. Simulation parameters for the cable attenuation to model the experiment.

Frequency (MHz)	1	10	50	100	200	400
$R_c(\sqrt{\omega/\omega_0}\Omega/m)$ Belden 8240	0.367	0.428	0.435	0.469	0.488	0.516
$R_c(\sqrt{\omega/\omega_0}\Omega/m)$ Belden 9201	0.496	0.471	0.509	0.523	0.527	0.564

been approximated in simulation as a linear interpolation function with the parameters in Table 2. For both cables analyzed, we find good agreement between experiments and theory, in both the level of the shielding effectiveness as well as the resonance frequency location.

It is our goal now to investigate if the use of multiple shields helps improve shielding effectiveness, and under what conditions. This is done in the next subsections in more detail.

3.2. Termination Effect and Losses Effect in Multiple-Shield Cables

Let's focus our attention on the 22-inch-long commercial Belden 8240 cable analyzed in Fig. 2. We now analyze a double-shield cable, where we introduce a second shield with the same parameters as the shield of the Belden 8240 cable. The braid outer and inner diameters are 0.134 and 0.116 inches, respectively, and the wire diameter is 0.005 inches. We compute the shielding effectiveness at $z = -11$ inch assuming a load of 0.5Ω at the inner conductor transmission line. Moreover, the inner shield transmission line is considered to be either shorted or matched. As shown in Fig. 5, when the inner shield transmission line is matched, the shielding effectiveness of such a double-shield cable is better than the single-shield cable in the entire frequency range analyzed. However, when it is shorted, an additional resonance around 260 MHz appears, where the cable behaves much worse than the single-shield cable. We believe that this resonance arises from the fact that the inter-shield region is a shorted transmission line of finite length, and the resonance is dictated by the permittivity of the dielectric between shields and the parameters of the shields. This is an important result to be taken into account for proper shielding engineering.

The cable attenuation is important to include at the resonances. We will include the cable attenuation by inserting center conductor losses $R_c = 0.43\sqrt{\omega/\omega_0}$ in Z_c [14], with $\omega_0 = 2\pi \times 10^7$ rad/s. We thus repeat the investigation of Fig. 5 including center conductor losses, and report the result in Fig. 6. It can be observed that the inclusion of R_c reduces the level of shielding effectiveness at 175 MHz only a few dBs, but leaves it unchanged in the remaining frequency range.

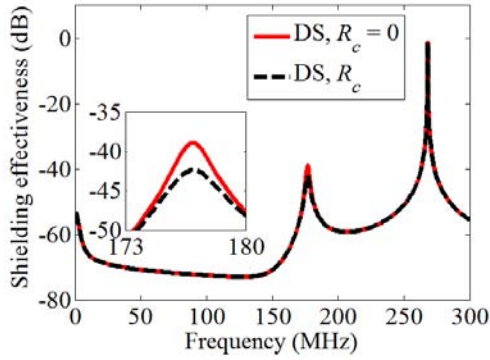


Figure 6. The shorted DS case in Fig. 5, but now considering center conductor losses $R_c = 0.43\sqrt{\omega/\omega_0}$.

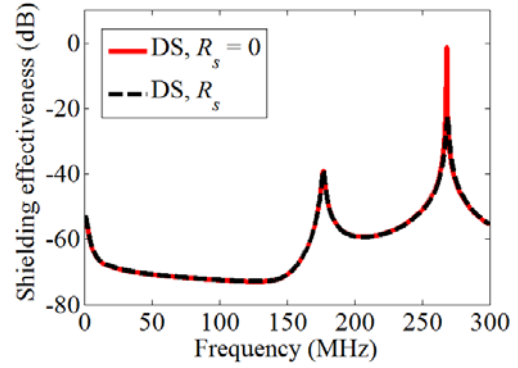


Figure 7. The shorted DS case in Fig. 5, but now considering the shield loss resistance.

Let's now take into account that the shields may have a non-negligible resistive component. We include the shield loss resistance and show the result in Fig. 7. We observe that now, in contrast to the center conductor losses, only the extra resonance at 260 MHz is affected by shield loss. This resistive component dampens the resonance at 260 MHz, limiting its quality factor. Even in this case, however, the double-shield cable has worse shielding effectiveness around 260 MHz than the single-shield version shown in Fig. 5. Note that without the shield losses (in this approximate model) the level of the 260 MHz resonance is not finite.

3.3. Sizing Effect in Double-Shield Cables

Here we show that the geometry of the shields can greatly affect the shielding effectiveness of double-shield cables. In particular, we modify the inner b_1 and outer b_0 radii of the braid (and necessarily change the distance between the shield conductors, and thereby their inductive and capacitive coupling) and plot the shielding effectiveness in Fig. 8 compared to the single-shield case. When the two shields are very close to each other, i.e., $b_0/b_1 \cong 1$, one can see that the cable behaves the same (the region below

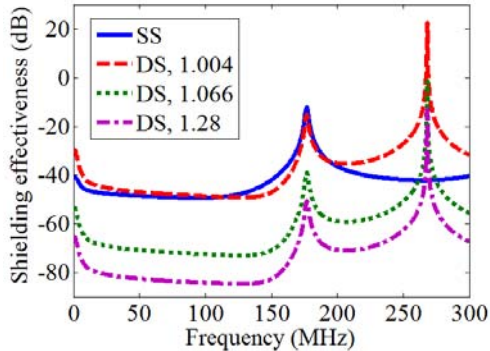


Figure 8. Shielding effectiveness for a 22-inch-long single- and double-shield cable computed at $z = -11$ inch assuming a load of 0.5Ω at the inner conductor transmission line. The inner shield transmission line is considered to be shorted. Shield radii dimensions are modified as detailed in the legend, which shows the ratio b_0/b_1 .

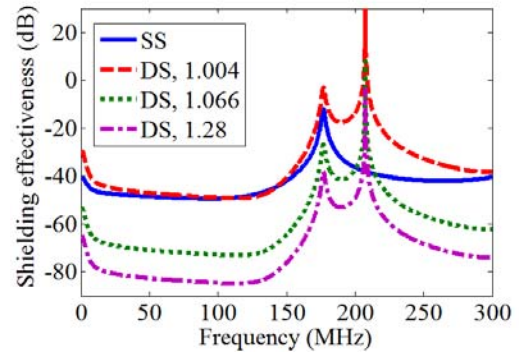


Figure 9. As in Fig. 8, but the permittivity between shields is modified from 1 to 1.67.

150 MHz) or worse than the single-shield one (the resonance region). Thus, little or no improvement is obtained by adding a second shield. Proper design and modeling is thus necessary to understand the proper effectiveness of shields, especially for applications where shielding is of vital importance. Increasing the distance between the shields leads to an overall improvement of the shielding effectiveness by more than 20 dB. Also in this case, however, the double-shield cable behaves worse than a single-shield one at 260 MHz.

We then modify the dielectric permittivity between the two shields to a value of 1.67, and replot in Fig. 9 the result observed in Fig. 8. As expected, this affects mostly the extra resonance at 260 MHz (due to the short circuit at the inner-shield transmission line) which is now moved to 210 MHz upon increase in dielectric contrast between the two shields.

4. CONCLUSION

In this paper we formulated a transmission-line model for calculating the shielding effectiveness of multiple-shield cables with arbitrary terminations. We have shown, with multiple examples, that increasing the number of shields of a cable may not improve the shielding performance. In particular, we observed that the shielding terminations are one of the main parameters to account for when designing shields.

ACKNOWLEDGMENT

We acknowledge T. L. Smith, Sandia National Laboratories, for the construction of Fig. 1(a). This work was supported in part by Sandia Corporation, a wholly owned subsidiary of Lockheed Martin Corporation, for the U.S. Department of Energy's National Nuclear Security Administration under contract DE-AC04-94AL85000.

REFERENCES

1. Schelkunoff, S. A., "The electromagnetic theory of coaxial transmission lines and cylindrical shields," *Bell System Technical Journal*, Vol. 13, 532–579, 1934.
2. Vance, E. F., *Coupling to Shielded Cables*, R. E. Krieger, 1987.
3. Lee, K. S. H., *EMP Interaction: Principles, Techniques, and Reference Data*, Hemisphere Publishing Corp., Washington, 1986.
4. Celozzi, S., R. Araneo, and G. Lovat, *Electromagnetic shielding*, John Wiley and Sons, 2008.
5. Tesche, F. M., M. V. Ianoz, and T. Karlsson, *EMC Analysis Methods and Computational Models*, John Wiley & Sons, Inc., New York, 1997.
6. Vance, E. F., "Shielding effectiveness of braided wire shields," *Interaction Note 172*, 1974.
7. Knowles, E. D. and L. E. Olson, "Cable shielding effectiveness testing," *IEEE Transactions on Electromagnetic Compatibility*, Vol. 16, 16–23, 1974.
8. Schulz, R. B., V. C. Plantz, and D. R. Brush, "Shielding theory and practice," *IEEE Transactions on Electromagnetic Compatibility*, Vol. 30, 187–201, 1988.
9. Jayasree, P. V. Y., V. S. S. N. S. Baba, B. Prabhakar Rao, and P. Lakshman, "Analysis of shielding effectiveness of single, double and laminated shields for oblique incidence of EM waves," *Progress In Electromagnetics Research B*, Vol. 22, 187–202, 2010.
10. Demoulin, B., P. Degauque, M. Cauterman, and R. Gabillard, "Shielding performance of triply shielded coaxial cables," *IEEE Transactions on Electromagnetic Compatibility*, Vol. 22, 173–180, 1980.
11. Kley, T., "Optimized single-braided cable shields," *IEEE Transactions on Electromagnetic Compatibility*, Vol. 35, 1–9, 1993.
12. Warne, L. K., W. L. Langston, L. I. Basilio, and W. A. Johnson, "Cable braid electromagnetic penetration model," *Sandia National Laboratories Report*, SAND2015-5019, Albuquerque, NM, 2015.

13. Warne, L. K., W. L. Langston, L. I. Basilio, and W. A. Johnson, "First principles cable braid electromagnetic penetration model," *Progress In Electromagnetics Research B*, Vol. 66, 63–89, 2016.
14. Hudson, H. G., S. L. Stronach, W. Derr, W. A. Johnson, L. K. Warne, J. Kotulski, et al., "Cable test system upgrade coaxial cable/connector model validation experiments," *Facility Test Report*, Albuquerque, NM, 2001.
15. Tyni, M., "The transfer impedance of coaxial cables with braided outer conductor," *FV. Nauk*, 410–419, Inst. Telekomum Akust. Politech Wroclaw, Ser. Konfi, 1975.
16. Warne, L. K., L. I. Basilio, W. L. Langston, K. C. Chen, H. G. Hudson, M. E. Morris, et al., "Electromagnetic coupling into two standard calibration shields on the Sandia cable tester," SAND2014-0842, Albuquerque, NM, 2014.